Dynamic phase transition in the kinetic spin-3/2 Blume–Emery–Griffiths model in an oscillating field

2006 J. Phys.: Condens. Matter 18 6635

(http://iopscience.iop.org/0953-8984/18/29/006)

INSTITUTE OF PHYSICS PUBLISHING JOURNAL OF PHYSICS: CONDENSED MATTER

J. Phys.: Condens. Matter **18** (2006) 6635–6653 doi:10.1088/0953-8984/18/29/006

Dynamic phase transition in the kinetic spin-3/2 Blume–Emery–Griffiths model in an oscillating field

Osman Canko, Bayram Deviren and Mustafa Keskin

Department of Physics, Erciyes University, 38039 Kayseri, Turkey

Received 21 April 2006, in final form 8 June 2006
Published 30 June 2006
Online at stacks.iop.org/JPhysCM/18/6635

Abstract

The dynamic phase transitions are studied, within a mean-field approach, in the kinetic Blume–Emery–Griffiths model under the presence of a time varying (sinusoidal) magnetic field by using the Glauber-type stochastic dynamics. The behaviour of the time-dependence of the order parameters and the behaviour of the average order parameters in a period, which is also called the dynamic order parameters, as a function of reduced temperature, are investigated. The nature (continuous and discontinuous) of transition is characterized by studying the average order parameters in a period. The dynamic phase transition points are obtained and the phase diagrams are presented in the reduced magnetic field amplitude and reduced temperature plane. The phase diagrams exhibit one, two, or three dynamic tricritical points and a dynamic double critical end point, and besides a disordered and two ordered phases, seven coexistence phase regions exist, which strongly depend on interaction parameters. We also calculate the Liapunov exponent to verify the stability of solutions and the dynamic phase transition points.

1. Introduction

Spin-3/2 Ising models have been paid much attention, which was first introduced [1] in connection to explaining the phase transition in $DyVO_4$. The most general spin-3/2 Ising model Hamiltonian with bilinear (J) and biquadratic (K) nearest-neighbour pair interactions and a single-ion potential or crystal-field interaction (D) is the spin-3/2 Blume–Emery–Griffiths (BEG) model. The spin-3/2 Ising Hamiltonian with only J and D interactions is known as the spin-3/2 Blume–Capel (BC) model and the spin-3/2 Ising Hamiltonian with only J and K interactions is known as the isotropic spin-3/2 (BEG) model. The equilibrium properties of the spin-3/2 BEG model for $K/J \geqslant 0$ have been studied and its phase diagrams have been calculated by renormalization-group (RG) techniques [2], the effective field theory (EFT) [3], the Monte Carlo (MC) simulation and a density-matrix-RG method [4]. An exact formulation of the spin-3/2 BEG model on a Bethe lattice was investigated by using the exact recursion

equations [5]. The ferromagnetic spin-3/2 BEG model with repulsive biquadratic coupling, i.e. $K/J < 0$, has also been investigated. An early attempt to study the ferromagnetic spin-3/2 BEG model was made by Barreto and Bonfim [6] and Bakkali *et al* [7] within the mean-field approximation (MFA) and also the MC calculation, and the EFT, respectively. Barreto and Bonfim [6], and Bakkali *et al* [7] presented two phase diagrams, one for the spin-3/2 BC model and one for the isotropic spin-3/2 BEG model. Tucker [8] studied the spin-3/2 BEG model with $K/J < 0$ by using the cluster variation method in pair approximation (CVMPA) and only presented the phase diagrams of the spin-3/2 BC and isotropic spin-3/2 BEG models for a few values of the coordination number. Bakchich and Bouziani [9] calculate the phase diagram of the model only in the $(T/J, D/J)$ plane for the two different values of K/J within an approximate renormalization-group approach of the Migdal–Kadanoff type. Ekiz *et al* [10] investigated the model on the Bethe lattice using the exact recursion equations and presented the phase diagrams in the $(kT/J, K/J)$ plane for several values of D/J and in the $(kT/J, D/J)$ plane for several values of K/J. Ekiz [11] extended the previous work, i.e., [10], for the presence of the external magnetic field. He considered only the ferromagnetic case. Recently, Keskin *et al* [12] studied the equilibrium behaviour of the antiferromagnetic spin-3/2 BEG model and presented the phase diagrams.

On the other hand, the ferromagnetic spin-3/2 BC model has been studied within the EFT [13], the MFA [14], the two-spin cluster approximation in the cluster expansion method [15], conventional finite-size-scaling, conformal invariance, and MC simulations [16], the pair approximation for the free energy and MC simulations [17], and a thermodynamically self-consistent theory based on an Ornstein–Zernike approximation [18] and extensive MC simulations [19]. The exact solution of the ferromagnetic spin-3/2 BC model was presented on the Bethe lattice by means of the exact recursion relations [20]. An early attempt to study the antiferromagnetic spin-3/2 BC model was made by Bakchich *et al* [21]. They examined the multicritical behaviour of the model with antiferromagnetic bilinear interaction, with a crystal field and under an external magnetic field by using the MFA. Bekhechi and Benyoussef [22] investigated the multicritical behaviour of the antiferromagnetic spin-3/2 BC model by using the transfer-matrix finite-size-scaling (TMFSS) calculations and MC simulations. Ekiz [23, 24] studied the antiferromagnetic spin-3/2 BC model on the Bethe lattice in an external magnetic field by using the recursion method. Recently, Keskin *et al* [25] studied the antiferromagnetic spin-3/2 BC model in an external magnetic field by the cluster variation method. Moreover, the dynamic aspect of the spin-3/2 BC model was made by Grandi and Figueiredo [26]. They employed the MC simulations and short-time dynamic scaling to determine the static and dynamic critical exponents for the two-dimensional spin-3/2 BC model and discussed critical exponents, extensively. Keskin *et al* [27] studied the dynamic phase transition in the kinetic spin-3/2 BC under presence of a time varying magnetic field by using the Glauber-type stochastic dynamic.

While the equilibrium properties of the spin-3/2 BEG model have been studied extensively, to our knowledge the nonequilibrium aspects of the spin-3/2 BEG model have not been investigated. The purpose of the present paper is, therefore, to study within the mean-field approach the stationary states of the kinetic spin-3/2 BEG model in the presence of a time-dependent oscillating external magnetic field. We use the Glauber-type stochastic dynamics to describe the time evolution of the system [28]. Especially, we investigate the time dependence of average magnetization and the behaviour of the dynamic order parameters as a function of the temperature. In these studies, we obtain the dynamical phase transition (DPT) points and construct the phase diagrams in the temperature and magnetic field amplitude plane. We also calculate the Liapunov exponent to verify the stability of solutions and the DPT points. This type of calculation was first applied to a kinetic spin-1/2 Ising system by Tomé

and Oliveira [29] and then used to study kinetics of a classical mixed spin-1/2 and spin-1 Ising system by Buendía and Machado [30], and kinetics of spin-1 Ising [31, 32] and spin-3/2 BC [27] models by Keskin *et al*.

We should also mention that the dynamic phase transition (DPT) is one of the characteristic behaviours in a nonequilibrium system in the presence of an oscillating external magnetic field and has been paid much attention in recent years. The DPT was first found in a study within a mean-field approach of the stationary states of the kinetic spin-1/2 Ising model under a time-dependent oscillating field [29, 33], by using the Glauber-type stochastic dynamics [28], and it was followed by Monte Carlo simulation, which allows the microscopic fluctuations, and research of kinetic spin-1/2 Ising models [34–37], as well as further mean-field studies [38]. Moreover, Tutu and Fujiwara [39] developed a systematic method for getting the phase diagrams in DPTs, and constructed the general theory of DPTs near the transition point based on mean-field description, such as Landau's general treatment of the equilibrium phase transitions. The DPT has also been found in a one-dimensional kinetic spin-1/2 Ising model with boundaries [40]. Experimental evidence for the DPT has been found in highly anisotropic (Ising-like) and ultrathin Co/Cu(001) ferromagnetic films [41] and in ferroic systems (ferromagnets, ferroelectrics and ferroelastics) with pinned domain walls [42]. Furthermore, we should also mention that recent research on the DPT has been widely extended to more complex systems such as vector type order parameter systems, e.g., the Heisenberg-spin systems [43], XY model [44], a Ziff–Gulari–Barshad model for CO oxidation with CO desorption to periodic variation of the CO pressure [45] and high-spin Ising models such as kinetics of spin-1 Ising [31, 32] and spin-3/2 BC [27] models, and a mixed-spin Ising model, e.g., the kinetics of a mixed spin-1/2 and spin-1 Ising model [30]. The DTP in model ferromagnetic systems (Ising and Heisenberg) in the presence of a sinusoidally oscillating magnetic field have been reviewed recently by Acharyya [46].

Finally, it is worthwhile to mention that the dynamic phase transition observed from the solution of a mean-field dynamical equation is not truly dynamic as it can exist for such equations of motion even in the zero frequency (static) limit of the driving field. This transition is an artifact of the mean-field approximation, which neglects nontrivial fluctuations. The reason is that the DPT can exist even in the static limit as follows. For field amplitudes less than the static coercive field h_C (which is nonzero below the ordered–disordered transition temperatures T_C), the response order parameters vary periodically but asymmetrically even in the zero frequency limit. The system then remains locked to the higher, yet locally attractive, well of the free energy and cannot go to the other (deeper) well, unless driven by any noise or fluctuations that are absent in the mean-field system [34, 36]. Although the numerical solution of the mean-field dynamical equations of motion cannot provide for a true dynamic phase transition, it is still important because it can be used to obtain some qualitative features of the dynamic phase transition. Moreover, the mean-field equation of the spin-1/2 Ising system can be linearized and this linearized equation is exactly solvable [46].

The outline of the remaining part of this paper is organized as follows. In section 2, the spin-3/2 BEG model is presented briefly. In section 3, the derivation of the mean-field dynamic equations of motion is given by using a Glauber-type stochastic dynamics in the presence of a time-dependent oscillating external magnetic field. In section 4, the stationary solutions of the coupled dynamic equations are solved and the thermal behaviours of the dynamic order parameters are studied, and as a result the DPT points are calculated. Moreover, we also calculate the Liapunov exponent to verify the stability of a solution and the DPT points. Section 5 contains the presentation and the discussion of the phase diagrams. Finally, a summary and discussion are given in section 6.

2. The model

The spin-3/2 BEG model, which is the most general spin-3/2 Ising model, has been paid much attention for many years. The model is described by the following Hamiltonian:

$$H = -J \sum_{\langle ij \rangle} S_i S_j - K \sum_{\langle ij \rangle} \left(S_i^2 - 5/4\right)\left(S_j^2 - 5/4\right) - \Delta \sum_i \left(S_i^2 - 5/4\right) - H \sum_i S_i, \tag{1}$$

where the S_i take the value $\pm 3/2$ or $\pm 1/2$ at each i site of a lattice and the summation index $\langle ij \rangle$ denotes a summation over all pairs of neighbouring spins. J and K are, respectively, the nearest-neighbour bilinear and biquadratic exchange constants, Δ is the crystal field interaction or single-ion anisotropy constant, and the last term, H, is a time-dependent external oscillating magnetic field. H is given by

$$H(t) = H_0 \cos(\omega t), \tag{2}$$

where H_0 and $\omega = 2\pi\nu$ are the amplitude and the angular frequency of the oscillating field, respectively. The system is in contact with an isothermal heat bath at absolute temperature.

The spin-3/2 BEG model is also a three-order-parameter system; these are introduced as follows. (1) The average magnetization $s = \langle S_i \rangle$, which is the excess of one orientation over the other orientation, also called the dipole moment. (2) The quadrupole moment q, that is a linear function of the average squared magnetization, i.e. $q = \langle S_i^2 \rangle - 5/4$, which is different from the definition $q \equiv \langle S_i^2 \rangle$ used in some research [3, 6–9]. The first definition ensures that $q = 0$ at infinite temperature. (3) The octupolar moment r, which is an odd function of the average magnetization $\langle S_i \rangle$ and defined as $r = 5/3 \langle S_i^3 \rangle - 41/12 \langle S_i \rangle$. This definition also ensures that $r = 0$ at infinite temperature and this is different from the definition $r = \langle S_i^3 \rangle$ used by some research [3, 7, 8]. We should also mention that since the behaviour of r is similar to the behaviour of s, we will not use r as many researchers have done.

3. Derivation of mean-field dynamic equations

Now, we apply the Glauber-type stochastic dynamics to obtain the mean-field dynamic equation of motion. Thus, the system evolves according to a Glauber-type stochastic process at a rate of $1/\tau$ transitions per unit time. We define $P(S_1, S_2, \ldots, S_N; t)$ as the probability that the system has the S-spin configuration, $S_1, S_2, \ldots, S_N$, at time t. The time-dependence of this probability function is assumed to be governed by the master equation which describes the interaction between spins and heat bath, and can be written as

$$\frac{\mathrm{d}}{\mathrm{d}t} P(S_1, S_2, \ldots, S_N; t) = -\sum_i \left(\sum_{S_i \neq S_i'} W_i(S_i \to S_i') \right) P(S_1, S_2, \ldots, S_i, \ldots, S_N; t)$$
$$+ \sum_i \left(\sum_{S_i \neq S_i'} W_i(S_i' \to S_i) P(S_1, S_2, \ldots, S_i', \ldots, S_N; t) \right), \tag{3}$$

where $W_i(S_i \to S_i')$, the probability per unit time that the ith spin changes from the value S_i to S_i', and in this sense the Glauber model is stochastic. Since the system is in contact with a heat bath at absolute temperature T, each spin can change from the value S_i to S_i' with the probability per unit time

$$W_i(S_i \to S_i') = \frac{1}{\tau} \frac{\exp\left(-\beta \Delta E(S_i \to S_i')\right)}{\sum_{S_i'} \exp\left(-\beta \Delta E(S_i \to S_i')\right)}, \tag{4}$$

where $\beta = 1/k_B T$, k_B is the Boltzmann factor, $\sum_{S_i'}$ is the sum over the four possible values of S_i', $\pm 3/2$, $\pm 1/2$ and

$$\Delta E(S_i \to S_i') = -(S_i' - S_i)\left(H + J\sum_{\langle j\rangle} S_j\right) - (S_i'^2 - S_i^2)\left(\Delta + K\sum_{\langle j\rangle}\left(S_j^2 - 5/4\right)\right), \quad (5)$$

gives the change in the energy of the system when the S_i-spin changes. The probabilities satisfy the detailed balance condition

$$\frac{W_i(S_i \to S_i')}{W_i(S_i' \to S_i)} = \frac{P(S_1, S_2, \ldots, S_i', \ldots, S_N)}{P(S_1, S_2, \ldots, S_i, \ldots, S_N)}, \quad (6)$$

and substituting the possible values of S_i we get

$$W_i\left(\tfrac{3}{2} \to -\tfrac{3}{2}\right) = W_i\left(\tfrac{1}{2} \to -\tfrac{3}{2}\right) = W_i\left(-\tfrac{1}{2} \to -\tfrac{3}{2}\right) = W_i\left(-\tfrac{3}{2} \to -\tfrac{3}{2}\right)$$
$$= \frac{1}{2\tau}\frac{\exp(-\beta y)\exp(-3\beta x/2)}{\exp(\beta y)\cosh(-3\beta x/2) + \exp(-\beta y)\cosh(-\beta x/2)}, \quad (7a)$$

$$W_i\left(\tfrac{3}{2} \to -\tfrac{1}{2}\right) = W_i\left(\tfrac{1}{2} \to -\tfrac{1}{2}\right) = W_i\left(-\tfrac{1}{2} \to -\tfrac{1}{2}\right) = W_i\left(-\tfrac{3}{2} \to -\tfrac{1}{2}\right)$$
$$= \frac{1}{2\tau}\frac{\exp(-\beta y)\exp(-\beta x/2)}{\exp(\beta y)\cosh(-3\beta x/2) + \exp(-\beta y)\cosh(-\beta x/2)}, \quad (7b)$$

$$W_i\left(\tfrac{3}{2} \to \tfrac{1}{2}\right) = W_i\left(\tfrac{1}{2} \to \tfrac{1}{2}\right) = W_i\left(-\tfrac{1}{2} \to \tfrac{1}{2}\right) = W_i\left(-\tfrac{3}{2} \to \tfrac{1}{2}\right)$$
$$= \frac{1}{2\tau}\frac{\exp(-\beta y)\exp(\beta x/2)}{\exp(\beta y)\cosh(-3\beta x/2) + \exp(-\beta y)\cosh(-\beta x/2)}, \quad (7c)$$

$$W_i\left(\tfrac{3}{2} \to \tfrac{3}{2}\right) = W_i\left(\tfrac{1}{2} \to \tfrac{3}{2}\right) = W_i\left(-\tfrac{1}{2} \to \tfrac{3}{2}\right) = W_i\left(-\tfrac{3}{2} \to \tfrac{3}{2}\right)$$
$$= \frac{1}{2\tau}\frac{\exp(\beta y)\exp(3\beta x/2)}{\exp(\beta y)\cosh(-3\beta x/2) + \exp(-\beta y)\cosh(-\beta x/2)}, \quad (7d)$$

where $x = H + J\sum_{\langle j\rangle} S_j$, $y = \Delta + K\sum_{\langle j\rangle}(S_j^2 - 5/4)$. Notice that, since $W_i(S_i \to S_i')$ does not depend on the value S_i, we can write $W_i(S_i \to S_i') = W_i(S_i')$, then the master equation becomes

$$\frac{\mathrm{d}}{\mathrm{d}t}P(S_1, S_2, \ldots, S_N; t) = -\sum_i\left(\sum_{S_i' \neq S_i} W_i(S_i')\right)P(S_1, S_2, \ldots, S_i, \ldots, S_N; t)$$
$$+ \sum_i W_i(S_i)\left(\sum_{S_i' \neq S_i} P(S_1, S_2, \ldots, S_i', \ldots, S_N; t)\right). \quad (8)$$

Since the sum of probabilities is normalized to one, by multiplying both sides of equation (8) by first S_k then $(S_k^2 - 5/4)$ and taking the average, we obtain

$$\tau\frac{\mathrm{d}}{\mathrm{d}t}\langle S_k\rangle = -\langle S_k\rangle + \left\langle\frac{3\exp(\beta y)\,\sinh(3\beta x/2) + \exp(-\beta y)\,\sinh(\beta x/2)}{2\exp(\beta y)\,\cosh(3\beta x/2) + 2\exp(-\beta y)\,\cosh(\beta x/2)}\right\rangle, \quad (9)$$

$$\tau\frac{\mathrm{d}}{\mathrm{d}t}\langle S_k^2 - 5/4\rangle = -\langle S_k^2 - 5/4\rangle + \left\langle\frac{\exp(\beta y)\,\cosh(3\beta x/2) - \exp(-\beta y)\,\cosh(\beta x/2)}{\exp(\beta y)\,\cosh(3\beta x/2) + \exp(-\beta y)\,\cosh(\beta x/2)}\right\rangle. \quad (10)$$

These dynamic equations can be written in terms of a mean-field approach and hence the set of the mean-field dynamical equations of the system in the presence of a time-varying field is

$$\tau\frac{\mathrm{d}}{\mathrm{d}t}\langle S\rangle = -\langle S\rangle + \left\langle \frac{3\exp(\beta a_1)\sinh(3\beta a_2/2) + \exp(-\beta a_1)\sinh(\beta a_2/2)}{2\exp(\beta a_1)\cosh(3\beta a_2/2) + 2\exp(-\beta a_1)\cosh(\beta a_2/2)} \right\rangle, \tag{11}$$

$$\tau\frac{\mathrm{d}}{\mathrm{d}t}\langle S^2 - 5/4\rangle = -\langle S^2 - 5/4\rangle + \left\langle \frac{\exp(\beta a_1)\ \cosh(3\beta a_2/2) - \exp(-\beta a_1)\cosh(\beta a_2/2)}{\exp(\beta a_1)\cosh(3\beta a_2/2) + \exp(-\beta a_1)\cosh(\beta a_2/2)} \right\rangle, \tag{12}$$

where $a_1 = \Delta + Kz\langle S^2 - 5/4\rangle$, $a_2 = Jz\langle S\rangle + H_0\cos(\omega t)$, and z is the coordination number. The system evolves according to the set of these coupled differential equations given by equations (11) and (12) that can be written in the form

$$\Omega\frac{\mathrm{d}}{\mathrm{d}\xi}m = -m + \frac{3\exp[(d+kq)/T]\sinh[3(m+h\cos\xi)/2T] + \exp[-(d+kq)/T]\sinh[(m+h\cos\xi)/2T]}{2\exp[(d+kq)/T]\cosh[3(m+h\cos\xi)/2T] + 2\exp[-(d+kq)/T]\cosh[(m+h\cos\xi)/2T]}, \tag{13}$$

$$\tau\frac{\mathrm{d}q}{\mathrm{d}t} = -q + \frac{\exp[(d+kq)/T]\cosh[3(m+h\cos\xi)/2T] - \exp[-(d+kq)/T]\cosh[(m+h\cos\xi)/2T]}{\exp[(d+kq)/T]\cosh[3(m+h\cos\xi)/2T] + \exp[-(d+kq)/T]\cosh[(m+h\cos\xi)/2T]}, \tag{14}$$

where $m \equiv \langle S\rangle$, $q \equiv \langle S^2\rangle - 5/4$, $\xi = \omega t$, $T = (\beta z J)^{-1}$, $k = K/J$, $d = \Delta/zJ$, $h = H_0/zJ$, $\Omega = \tau\omega$. Hence, the set of the mean-field dynamical equations for the order parameters is obtained. We fixed $z = 4$ and $\Omega = 2\pi$. The solution and discussion of this equation are given in the next section.

4. Thermal behaviours of dynamic order parameters and dynamic phase transition points

In this section, we shall first solve the set of dynamic equations and present the behaviours of average order parameters in a period as a function of the reduced temperature, and as a result the DPT points are calculated. Moreover, we also calculate the Liapunov exponents to verify the stability of solutions and the dynamic phase transition points. For these purposes, first we have to study the stationary solutions of the set of dynamic equations, given in equations (13) and (14), when the parameters T, k, d and h are varied. The stationary solutions of equations (13) and (14) will be a periodic function of ξ with period 2π; that is, $m(\xi + 2\pi) = m(\xi)$ and $q(\xi + 2\pi) = q(\xi)$. Moreover, they can be one of three types according to whether they have or do not have the property

$$m(\xi + \pi) = -m(\xi), \tag{15a}$$

and

$$q(\xi + \pi) = -q(\xi). \tag{15b}$$

A solution that satisfies both equations (15*a*) and (15*b*) is called a symmetric solution, which corresponds to a disordered (D) solution. In this solution, the magnetization $m(\xi)$ always oscillates around the zero value and is delayed with respect to the external magnetic field. On the other hand, the quadrupolar order parameters $q(\xi)$ oscillate around a non-zero value for finite temperatures and around a zero value for the infinite temperature due to the reason that $q = 0$ at the infinite temperature by the definition of q, given in section 2. The second type of solution, which does not satisfy equations (15*a*) and (15*b*), is called a nonsymmetric solution, that corresponds to a ferromagnetic solution. In this case the magnetization and quadrupolar order parameters do not follow the external magnetic field any more, but instead of oscillating around a zero value; they oscillate around a nonzero value, namely $m(\xi)$ oscillates around either $\pm 3/2$ or $\pm 1/2$. Hence, if it oscillates around $\pm 3/2$, this nonsymmetric solution corresponds to the ferromagnetic $\pm 3/2$ ($\mathrm{F}_{3/2}$) phase and if it oscillates around $\pm 1/2$, this corresponds to the ferromagnetic $\pm 1/2$ ($\mathrm{F}_{1/2}$) phase. The third type of solution, which does satisfy equation (15*a*) but does not satisfy equation (15*b*), corresponds to ferroquadrupolar or simply quadrupolar

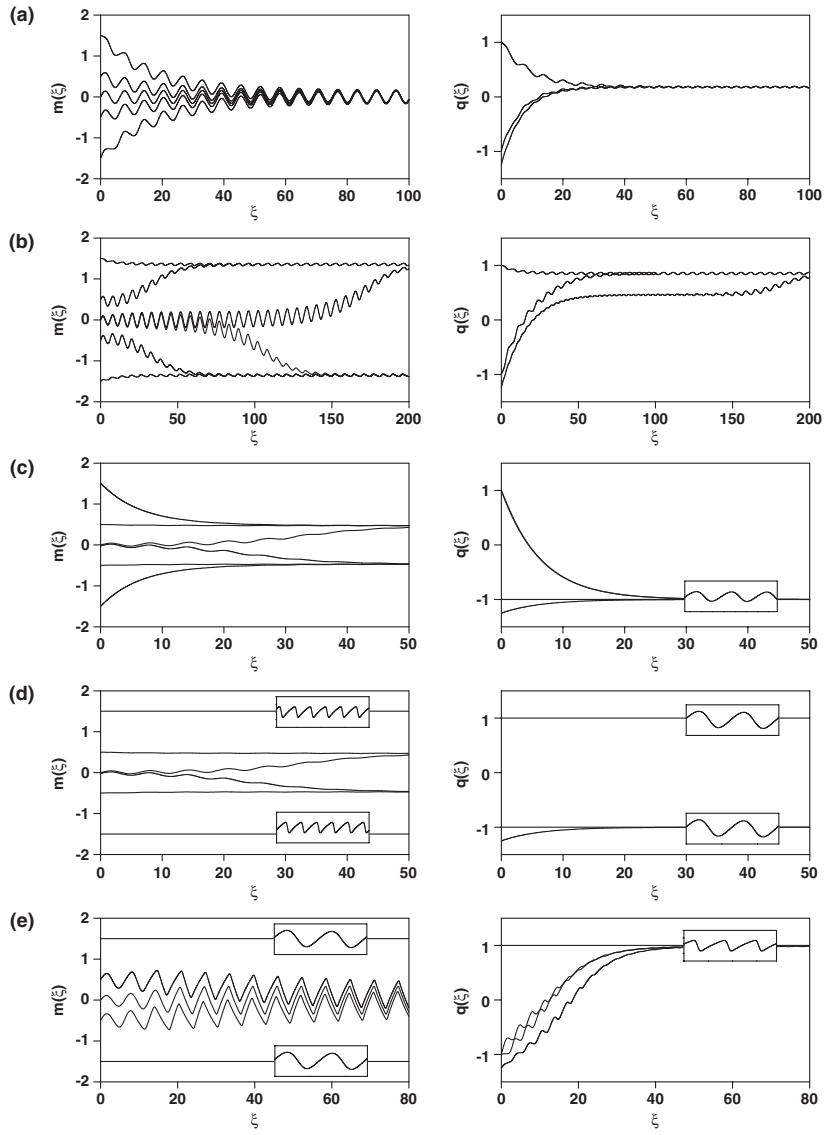

Figure 1. Time variations of the magnetization (m) and the quadrupolar order parameter (q): (a) exhibiting a disordered phase (D), $k = 0.1$, $d = 0.50$, $h = 1.50$, and $T = 1.50$. (b) Exhibiting a ferromagnetic phase-3/2 ($F_{3/2}$), $k = 1.0$, $d = 0.75$, $h = 0.50$, and $T = 1.0$. (c) Exhibiting a ferromagnetic phase-1/2 ($F_{1/2}$), $k = 0.5$, $d = 1.25$, $h = 0.25$, and $T = 0.125$. (d) Exhibiting a coexistence region ($F_{3/2} + F_{1/2}$), $k = 0.1$, $d = -0.50$, $h = 0.125$, and $T = 0.125$. (d) Exhibiting a coexistence region ($F_{3/2} + D$), $k = 2.0$, $d = 1.25$, $h = 1.25$, and $T = 0.25$. (e) Exhibiting a coexistence region ($F_{3/2}+F_{1/2}+FQ$), $k = 0.5$, $d = -0.125$, $h = 0.4$, and $T = 0.05$. (f) Exhibiting a coexistence region ($F_{3/2} + FQ$), $k = 1.0$, $d = 0.125$, $h = 0.50$, and $T = 0.50$. (g) Exhibiting a coexistence region ($F_{1/2} + FQ$), $k = 0.1$, $d = -1.0$, $h = 0.45$, and $T = 0.05$. (h) Exhibiting a coexistence region ($F_{3/2} + FQ + D$), $k = 0.5$, $d = -0.25$, $h = 1.25$, and $T = 0.10$. (i) Exhibiting a coexistence region ($FQ + D$), $k = 2.0$, $d = -0.125$, $h = 2.0$, and $T = 0.5$.

(FQ) phase. In this solution, $m(\xi)$ oscillates around the zero value and is delayed with respect to the external magnetic field and $q(\xi)$ does not follow the external magnetic field any more; but instead of oscillating around a zero value it oscillates around a nonzero value, namely

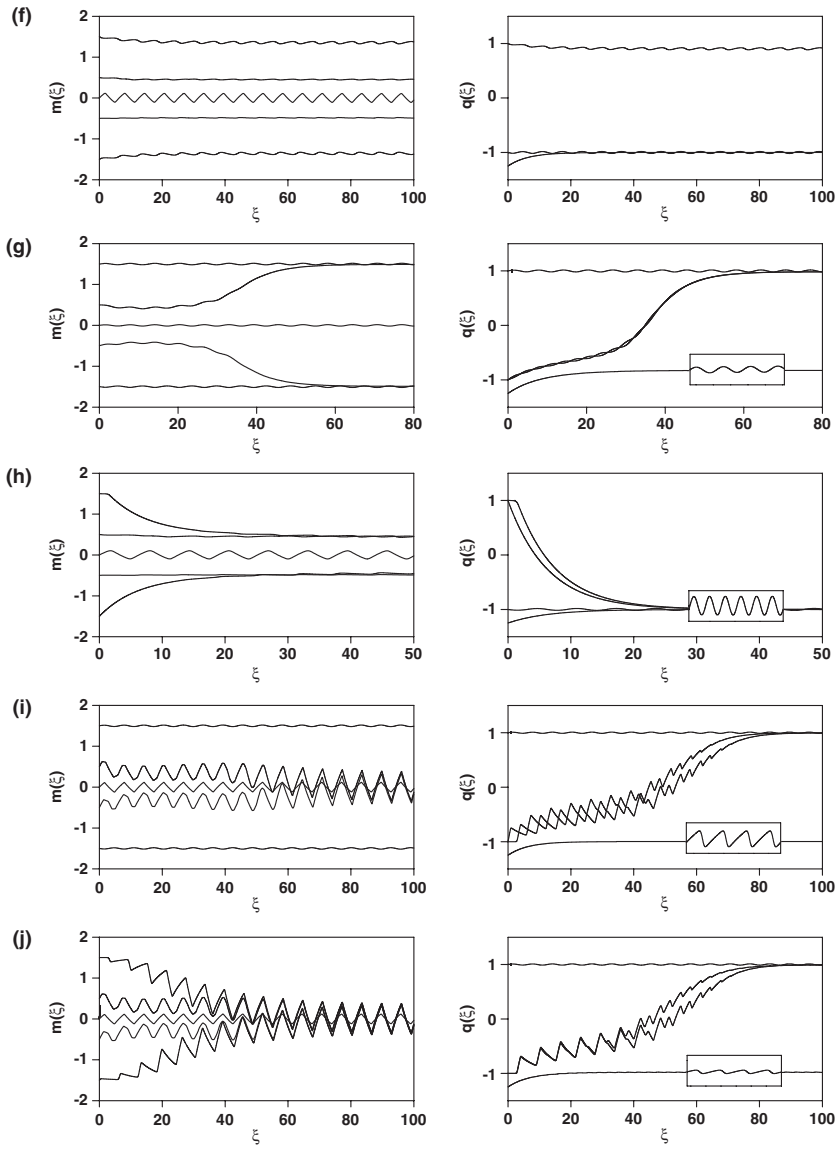

Figure 1. (Continued.)

either -1 or $+1$. Hence if it oscillates around -1 this nonsymmetric solution corresponds to the ferroquadrupolar or simply quadrupolar (FQ) phase, and if it oscillates around $+1$ this corresponds to the disordered phase (D). These facts are seen explicitly by solving equations (13) and (14) numerically. Equations (13) and (14) are solved by using the numerical method of the Adams–Moulton predictor corrector method for a given set of parameters and initial values and presented in figure 1. From figure 1, one can see ten different solutions, namely the D, $F_{3/2}$, and $F_{1/2}$ phases or solutions and seven coexistence solutions, namely the $F_{3/2}+F_{1/2}$ in which $F_{3/2}$ and $F_{1/2}$ solutions coexist, the $F_{3/2}+D$ in which $F_{3/2}$ and D solutions coexist, the $F_{3/2}+FQ$ in which $F_{3/2}$ and FQ solutions coexist, the $F_{1/2}+FQ$ in which $F_{1/2}$ and

FQ solutions coexist, the $F_{3/2} + F_{1/2} + FQ$ in which $F_{3/2}$, $F_{1/2}$, and FQ solutions coexist, the $F_{3/2} + FQ + D$ in which $F_{3/2}$, FQ, and D solutions coexist, and the $FQ + D$ in which FQ and D solutions coexist. In figure 1(a) only the symmetric solution is always obtained, hence we have a disordered (D) solution, but in figures 1(b) and (c) only the nonsymmetric solutions are found; therefore, we have the $F_{3/2}$ and $F_{1/2}$ solutions, respectively. These solutions do not depend on initial values. In figure 1(d), we have nonsymmetric solutions for $m(\xi)$ and $q(\xi)$, because $m(\xi)$ oscillates around either $\pm 3/2$ or $\pm 1/2$ values and $q(\xi)$ around $+1$ or -1, respectively, hence we have the coexistence solution ($F_{3/2} + F_{1/2}$). In figure 1(e), $m(\xi)$ oscillates around either $\pm 3/2$ or zero values and $q(\xi)$ around $+1$; as explained above, the solution of $m(\xi)$ oscillates around zero values and $q(\xi)$ around nonzero values corresponds to the D phase, because $q(\xi)$ is around $+1$ or nonzero values for low temperatures but around zero values for high temperatures. Therefore, we have the coexistence solution ($F_{3/2} + D$). In figure 1(f), $m(\xi)$ oscillates around $\pm 3/2$, $q(\xi)$ around $+1$, and $m(\xi)$ oscillates around $\pm 1/2$ or zero values, $q(\xi)$ around -1, hence we have the coexistence solution ($F_{3/2} + F_{1/2} + FQ$). Similarly, in figures 1(g)–(j) we have the $F_{3/2} + FQ$, $F_{1/2} + FQ$, $F_{3/2} + FQ + D$, and $FQ + D$ coexistence solutions, respectively. We should also mention that the solutions shown in figures 1(d)–(j) depend on the initial values.

Thus, figure 1 displays that we have ten phases in the system, namely D, $F_{3/2}$, $F_{1/2}$, $F_{3/2} + F_{1/2}$, $F_{3/2} + D$, $F_{3/2} + F_{1/2} + FQ$, $F_{3/2} + FQ$, $F_{1/2} + FQ$, $F_{3/2} + FQ + D$, and $FQ + D$ solutions or phases. In order to see the dynamic phase boundaries among these ten phases, we have to calculate DPT points and then we can present phase diagrams of the system. DPT points will be obtained by investigating the behaviour of the average order parameters in a period or the dynamic order parameters as a function of the reduced temperature. These investigations will also be checked and verified by calculating the Liapunov exponents.

The dynamic order parameters, namely the dynamic magnetization (M) and the dynamic quadruple moment (Q), are defined as

$$M = \frac{1}{2\pi} \int_0^{2\pi} m(\xi)\, \mathrm{d}\xi, \tag{16}$$

$$Q = \frac{1}{2\pi} \int_0^{2\pi} q(\xi)\, \mathrm{d}\xi. \tag{17}$$

The behaviour of M and Q as a function of the reduced temperature for several values of k, d, and h are obtained by combining the numerical methods of Adams–Moulton predictor corrector with the Romberg integration. We gave explanatory a few interesting examples to illustrate the calculation of the DPT and the dynamic phase boundaries among ten phases, seen in figures 2(a)–(e). In the figures, thick and thin lines represent M and Q, respectively; T_C and T_t are the critical or the second-order phase transition and first-order phase transition temperatures for both M and Q, respectively. Figures 2(a) and (b) show the behaviour of M and Q as a function of the reduced temperature for $k = 0.1$, $d = -0.375$, and $h = 0.125$ for three different initial values; i.e., the initial values of M and Q are taken as $3/2$ and 1.0, respectively, for figure 2(a), and $M = 1/2$ and $Q = -1.0$ or $M = 0$ and $Q = -1.25$ for figure 2(b). In figure 2(a), $M = 3/2$ and $Q = 1.0$ at zero temperature and M decreases to zero continuously as the reduced temperature increases, hence the system exhibits a second-order phase transition. The phase transition is from the $F_{3/2}$ phase to the D phase. On the other hand, Q decreases until T_C, as the temperature increases, and at T_C, it makes a cusp and then increases again; finally, it becomes zero at infinite temperature. In figure 2(b), $M = 1/2$ and $Q = -1.0$ at zero temperature, the system undergoes two successive phase transitions: the first one is a first-order phase transition, because M and Q increase to $3/2$ and 1.0, respectively, discontinuously as the temperature increases and the temperature where the discontinuity occurs is the first-order phase transition temperature, T_t; the transition is from the $F_{1/2}$ phase to the $F_{3/2}$ phase.

The second one is a second-order phase transition from the $F_{3/2}$ phase to the D phase. From figures 2(a) and (b), one can see that the $F_{3/2} + F_{1/2}$ coexistence phase region also exists in the system; compare figures 2(a) and (b) with figure 4(d). Figures 2(c)–(e) illustrate the thermal variations of M and Q for $k = 0.1$, $d = -0.375$, and $h = 0.375$ for three different initial values, i.e. the initial values $M = 3/2$, $Q = 1.0$ for figure 2(c), $M = 1/2$ and $Q = -1.0$ for figure 2(d), and $M = 0$ and $Q = -1.0$ for figure 2(e). The behaviour of figure 2(c) is similar to figure 2(a), hence the system undergoes a second-order phase transition from the $F_{3/2}$ phase to the D phase. The behaviour of figure 2(d) is similar to figure 2(b), therefore the system undergoes two successive phase transitions and thus the $F_{3/2} + F_{1/2}$ coexistence phase region also exists in the system. In figure 2(e), $M = 0$ and $Q = -1.0$ at zero temperature and the system undergoes two successive phase transitions: the first one is a first-order phase transition from the FQ phase to the $F_{3/2}$ phase and the second one is a second-order phase transition from the $F_{3/2}$ phase to the D phase. From figures 2(c)–(e), one can see that the $F_{3/2} + F_{1/2} +$ FQ coexistence phase region also exists in the system; compare figures 2(c)–(e) with figure 4(d).

Now we can check and verify the stability of solutions, as well as the DPT points by calculating the Liapunov exponents. If we write equations (16) and (17) as

$$\Omega \frac{\mathrm{d}m}{\mathrm{d}\xi} = F_1(m, \xi), \tag{18}$$

$$\Omega \frac{\mathrm{d}q}{\mathrm{d}\xi} = F_2(q, \xi), \tag{19}$$

then the Liapunov exponents λ_m and λ_q are given by

$$\Omega\lambda_m = \frac{1}{2\pi}\int_0^{2\pi} \frac{\partial F_1}{\partial m}\mathrm{d}\xi, \tag{20}$$

$$\Omega\lambda_q = \frac{1}{2\pi}\int_0^{2\pi} \frac{\partial F_2}{\partial q}\mathrm{d}\xi. \tag{21}$$

The solutions are stable when $\lambda_m < 0$ and $\lambda_q < 0$. We have two Liapunov exponents, namely, one is associated with the symmetric solution, λ_{ms} and λ_{qs}, and the other with the nonsymmetric solution, λ_{mn} and λ_{qn}, for both m and q. If λ_{ms} and λ_{mn} increase to zero continuously as the reduced temperature approaches the phase transition temperature, the temperature where $\lambda_{mn} = \lambda_{ms} = 0$ is the second-order phase transition temperature, T_C. Moreover, λ_{qn} and λ_{qs} increase continuously as the reduced temperature approaches the phase transition temperature and the temperature where λ_{qn} and λ_{qs} make a cusp is the second-order phase transition temperature, T_C. The reason λ_{qn} and λ_{qs} are not zero at T_C is that Q is not zero at T_C and it is zero at infinite temperature. On the other hand, if the Liapunov exponents approach the phase transition temperature, the temperature at which the Liapunov exponents make a jump discontinuity is the first-order phase transition temperature. In order to see these behaviours explicitly, the values of the Liapunov exponents are calculated and plotted as a function of the reduced temperature for $k = 0.1$, $d = -0.375$, and $h = 0.125$ for two different initial values; i.e., the initial values of M and Q are taken as $3/2$ and 1.0 for figure 3(a) and $M = 1/2$ and $Q = -1$ for figure 3(b), respectively. These values correspond to figures 2(a) and (b), respectively. In the figures, thick and thin lines represent λ_s and λ_n, respectively, and T_C is the second-order phase transition temperature and T_t is the first-order phase transition temperature. In figure 3(a), the system undergoes a second-order phase transition, because $\lambda_{mn} = \lambda_{ms} = 0$ at $T_C = 0.705$ (λ_{mn} and λ_{ms} correspond to the $F_{3/2}$ phase and D phase, respectively). On the other hand, λ_{qn} and λ_{qs} make a cusp at T_C (λ_{qn} and λ_{qs} correspond to the $F_{3/2}$ and D phases, respectively). Figure 3(b) shows that the system exhibits two successive phase transitions. The first one is a first-order, because the Liapunov exponents make a jump discontinuity, hence

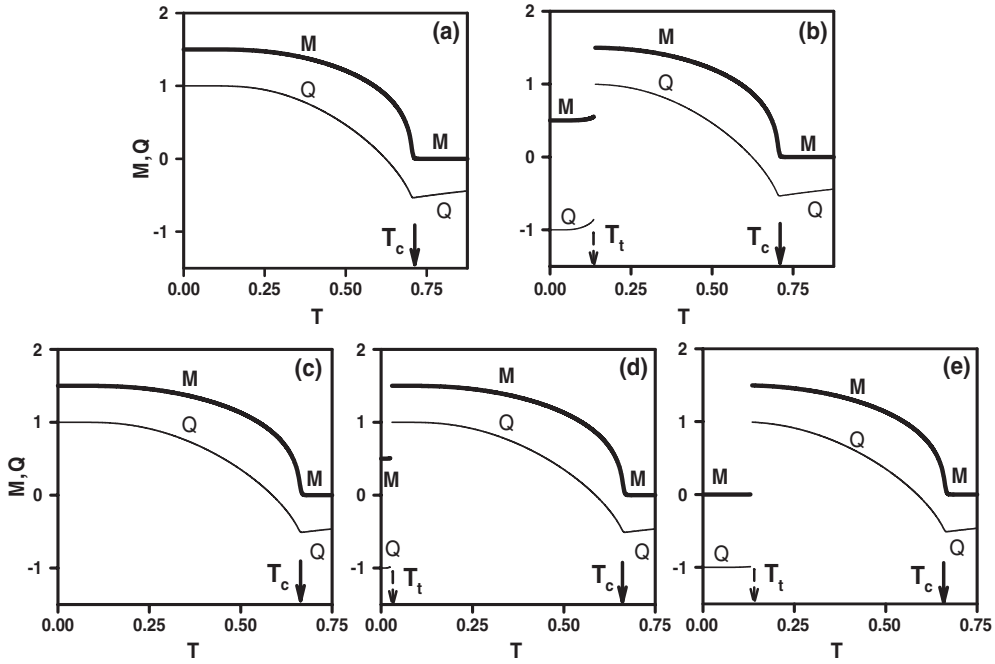

Figure 2. The reduced temperature dependence of the dynamic magnetization M and (the thick solid line) and the dynamic quadruple moment (Q) (the thin solid line). T_C and T_t are the critical or the second-order phase transition and the first-order phase transition temperatures for both M and Q, respectively. (a) Exhibiting a second-order phase transition from the $F_{3/2}$ phase to the D phase for $k = 0.1$, $d = -0.375$, and $h = 0.125$; 0.705 is found for T_C; (b) exhibiting two successive phase transitions; the first is a first-order one from the $F_{1/2}$ phase to the $F_{3/2}$ phase, the second is a second-order one from the $F_{3/2}$ phase to the D phase for $k = 0.1$, $d = -0.375$, and $h = 0.125$; 0.15 and 0.705 found for T_t and T_C respectively. (c) Exhibiting a second-order phase transition from the $F_{3/2}$ phase to the D phase for $k = 0.1$, $d = -0.375$, and $h = 0.375$; 0.685 is found for T_C. (d) Exhibiting two successive phase transitions; the first is a first-order one from the $F_{1/2}$ phase to the $F_{3/2}$ phase, the second is a second-order one from the $F_{3/2}$ phase to the $F_{3/2}$ to the D phase for $k = 0.1$, $d = -0.375$, and $h = 0.375$; 0.025 and 0.685 found for T_t and T_C respectively. (e) Exhibiting two successive phase transitions; the first is a first-order one from the FQ phase to the $F_{3/2}$, the second is a second-order one from the $F_{3/2}$ phase to the D phase for $k = 0.1$, $d = -0.375$, and $h = 0.375$; 0.135 and 0.685 found for T_t and T_C respectively.

the first-order phase transition temperature occurs at $T_t = 0.150$ ($\lambda_{mn'}$ and $\lambda_{qn'}$ correspond to the $F_{1/2}$ phase). The second one is the second-order phase transition at $T_C = 0.705$, which is similar to figure 3(a). If one compares figures 3(a) and (b) with figures 2(a) and (b), respectively, one can see that T_C and T_t found by using both calculations are exactly the same. Moreover, we have also verified the stability of the solution by this calculation, because we have always found that $\lambda_m < 0$ and $\lambda_q < 0$.

Finally, as mentioned before, the DPT, observed from the solution of the mean-field dynamical equations, is not truly dynamic. This is because for field amplitude less than the coercive field h_C (which is nonzero below the order–disorder transition temperature, T_C), the response order parameters vary periodically but asymmetrically even in the zero frequency limit; the system remains locked to one well of the free energy and cannot go to the other one, in the absence of noise or fluctuations [34, 36].

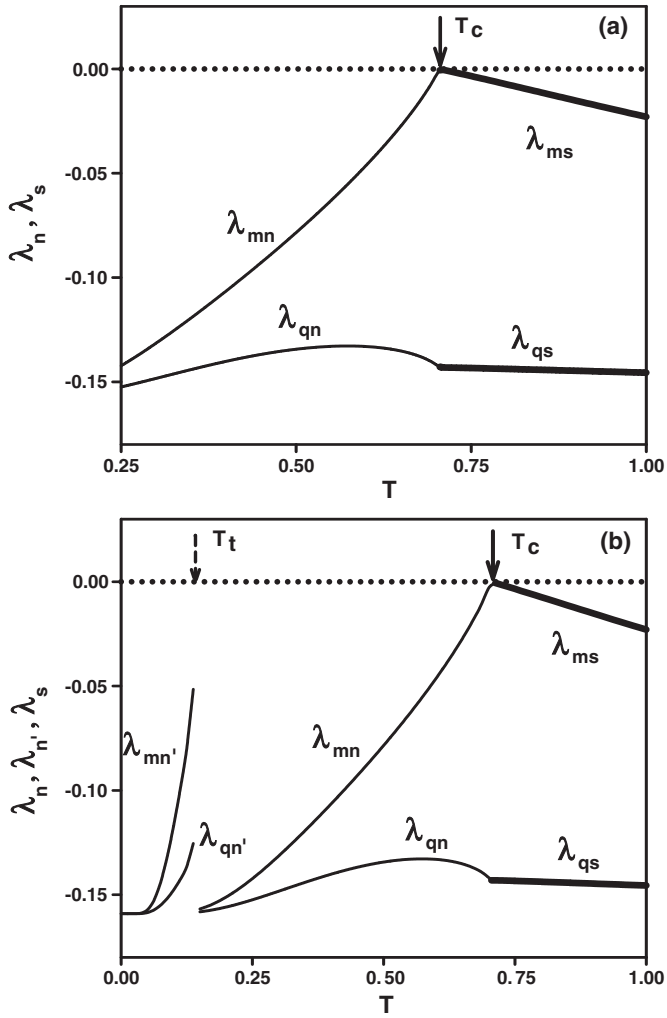

Figure 3. The values of the Liapunov exponents as a function of the reduced temperature (T) for $k = 0.1$, $d = -1.5$, and $h = 0.5$. Thick and thin lines represent the λ_s and λ_n, $\lambda_{n'}$, respectively, T_{C} are the critical or the second-order phase transition for both M and Q, and T_{t} is the first-order phase transition temperatures for M and Q. (a) For the initial values M and Q are taken as $3/2$ and 1.0, respectively. The system undergoes a second-order phase transition, because $\lambda_{mn} = \lambda_{ms} = 0$ at $T_{\mathrm{C}} = 0.705$ (λ_{mn} and λ_{ms} correspond to the $\mathrm{F}_{3/2}$ and D phases, respectively). λ_{qn} and λ_{qs} make a cusp, hence the second-order phase transition temperature occurs at $T_{\mathrm{C}} = 0.705$ (λ_{qn} and λ_{qs} correspond to the $\mathrm{F}_{3/2}$ and D phases, respectively). (b) For the initial values M and Q are taken as $1/2$ and -1.0 and/or 0 and -1.25, respectively. The system undergoes two successive phase transitions: the first one is first order, because the Liapunov exponents make a jump discontinuity at $T_{\mathrm{t}} = 0.15$ and the second one is second order, because $\lambda_{mn} = \lambda_{ms} = 0$; λ_{qn} and λ_{qs} make a cusp at $T_{\mathrm{C}} = 0.705$ ($\lambda_{mn'}$ and $\lambda_{qn'}$ correspond to the $\mathrm{F}_{1/2}$ phase, λ_{mn} and λ_{qn} correspond to the $\mathrm{F}_{3/2}$ phase, λ_{ms} and λ_{qs} correspond to the D phase).

5. Phase diagrams

Since we have obtained and verified the DPT points in section 4, we can now present the phase diagrams of the system. The calculated phase diagrams in the (T, h) plane are presented

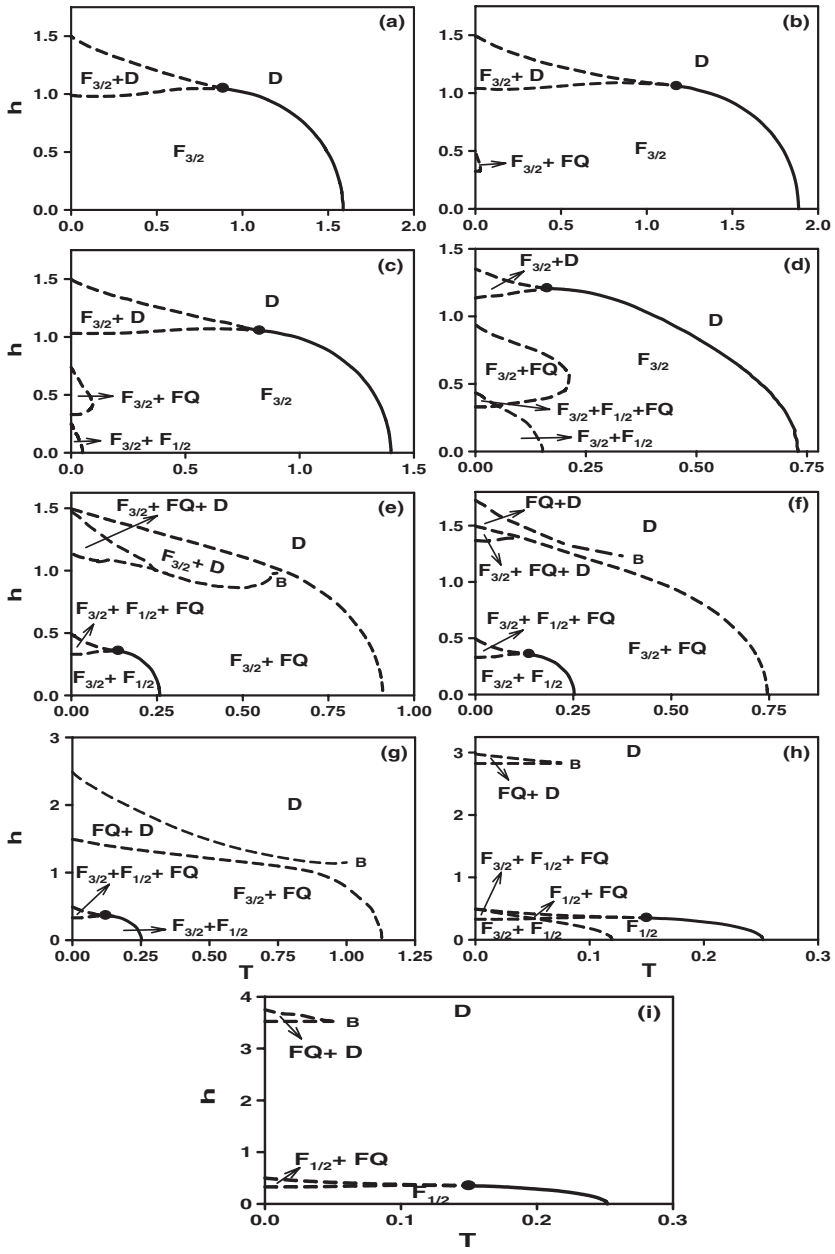

Figure 4. Phase diagrams of the spin-3/2 BEG model Hamiltonian with arbitrary bilinear and biquadratic pair interactions in the (T, h) plane, exhibiting one dynamic tricritical point. The disordered (D), ferromagnetic-3/2 ($F_{3/2}$), ferromagnetic-1/2 ($F_{1/2}$), and seven different coexistence regions, namely the $F_{3/2}+F_{1/2}$, $F_{3/2}+D$, $F_{3/2}+F_{1/2}+FQ$, $F_{3/2}+FQ$, $F_{1/2}+FQ$, $F_{3/2}+FQ+D$, and FQ + D regions, are found. Dashed and solid lines represent the first- and second-order phase transitions, respectively, the dynamic tricritical point is indicated with filled circles, and B denotes the dynamic double critical end point. (a) $k = 0.1$, $d = 0.5$, (b) $k = 1.0$, $d = 0.75$, (c) $k = 0.5$, $d = 0.125$, (d) $k = 0.1$, $d = -0.375$, (e) $k = 0.5$, $d = -0.25$, (f) $k = 0.5$, $d = -0.375$, (g) $k = 1.0$, $d = -0.25$, (h) $k = 0.5$, $d = -1.0$, and (i) $k = 0.5$, $d = 1.25$.

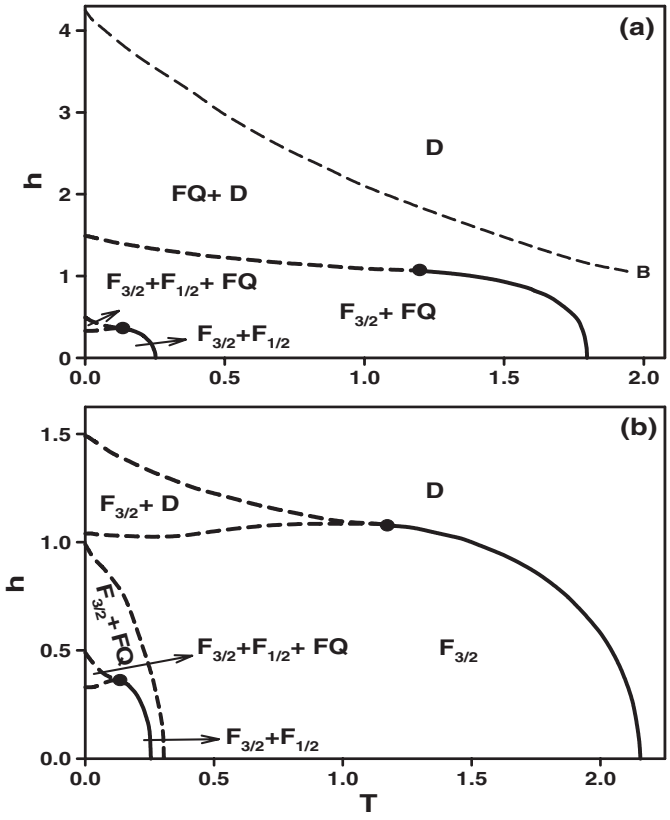

Figure 5. Phase diagrams of the spin-3/2 BEG model Hamiltonian with arbitrary bilinear and biquadratic pair interactions in the (T, h) plane, exhibiting two dynamic tricritical points. The disordered (D), ferromagnetic-3/2 ($F_{3/2}$), and five different coexistence regions, namely the $F_{3/2} + F_{1/2}$, $F_{3/2} + FQ$, $F_{3/2} + F_{1/2} + FQ$, $F_{3/2} + D$, and $FQ + D$ regions, are found. Dashed and solid lines represent the first- and second-order phase transitions, respectively, the dynamic tricritical points are indicated with filled circles, and B denotes the dynamic double critical end point. (a) $k = 2.0$, $d = -0.125$, (b) $k = 2.0$, $d = 1.25$.

in figures 4–6 for various values of k and d. In these phase diagrams, the solid and dashed lines represent the second-and the first-order phase transition lines, respectively, the dynamic tricritical point is denoted by a filled circle, and B represents the double critical end point. As seen from the figures, one, two or three dynamic tricritical points occur.

In figure 4, only one dynamic tricritical point exists and the following nine main topological different types of phase diagrams are found. (i) For $k = 0.1$ and $d = 0.50$, figure 4(a) represents the phase diagram in the (T, h) plane. In this phase diagram, at high reduced temperature (T) and reduced external magnetic field (h) the solutions are disordered (D) and at low values of T and h they are ferromagnetic-3/2 ($F_{3/2}$). The dynamic phase boundary between these regions, $F_{3/2} \rightarrow D$, is the second-order phase transition line. At low reduced temperatures, there is a range of values of h in which the D and the $F_{3/2}$ phases or regions coexist, called the coexistence region, $F_{3/2} + D$. The $F_{3/2} + D$ region is separated from the $F_{3/2}$ and the D phases by the first-order phase transition line. The system also exhibits only one dynamic tricritical point where both first-order phase transition lines merge and which signals the change from the first- to the second-order phase transition. Finally, we should

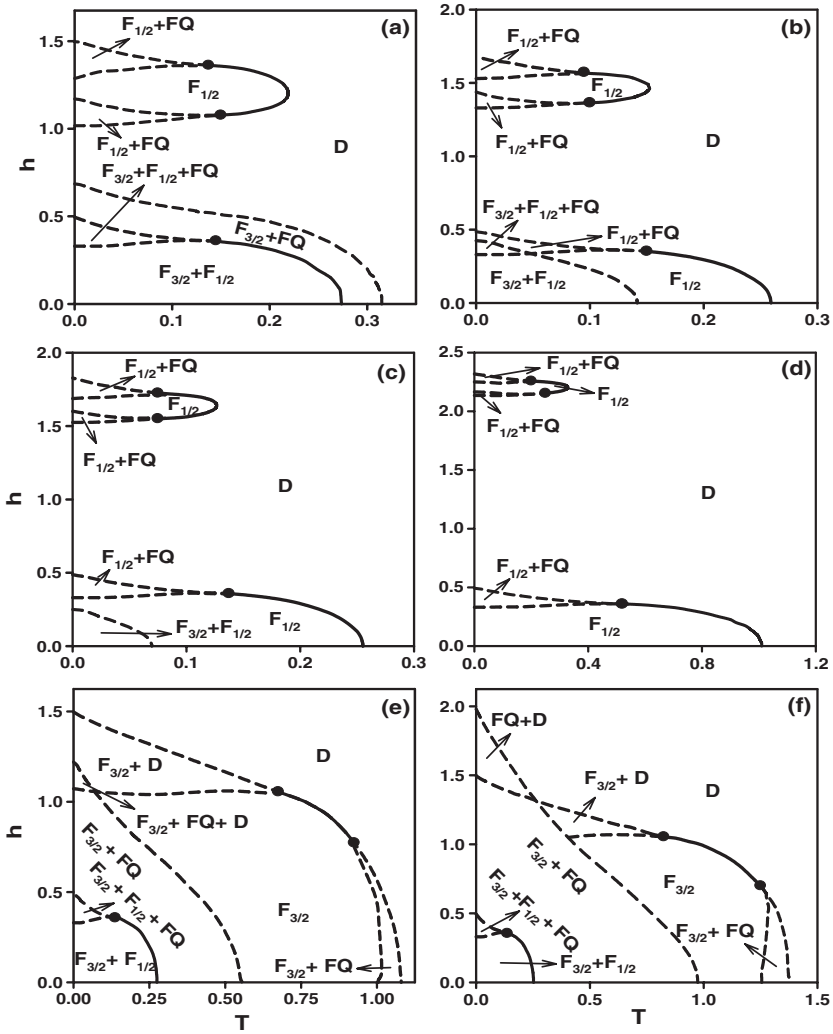

Figure 6. Phase diagrams of the spin-3/2 BEG model Hamiltonian with arbitrary bilinear and biquadratic pair interactions in the (T, h) plane, exhibiting three dynamic tricritical points. The disordered (D), ferromagnetic-3/2 ($F_{3/2}$), ferromagnetic-1/2 ($F_{1/2}$), and seven different coexistence regions, namely the $F_{3/2}+F_{1/2}$, $F_{3/2}+FQ$, $F_{1/2}+FQ$, $F_{3/2}+D$, $F_{3/2}+F_{1/2}+FQ$, $F_{3/2}+FQ+D$, and $FQ+D$ regions, are found. Dashed and solid lines represent the first- and second-order phase transitions, respectively, and the dynamic tricritical points are indicated with filled circles. (a) $k = 0.1$, $d = -0.5$, (b) $k = 0.1$, $d = -0.625$, (c) $k = 0.1$, $d = -0.7125$, (d) $k = 0.1$, $d = -1.0$, (e) $k = 0.5$, $d = -0.125$, and (f) $k = 1.0$, $d = 0.125$.

also mention that very similar phase diagrams were also obtained in the kinetic spin-1/2 Ising model [11], kinetic spin-1 BC model [10], kinetics of the mixed spin-1/2 and spin-1 Ising ferrimagnetic system [12], and as well in the kinetic spin-3/2 BC model [16]. This fact can be explicitly seen from the ground state phase diagrams of these three models. (ii) This type of phase diagram is presented for $k = 1.0$ and $d = 0.75$, seen in figure 4(b), and is similar to figure 4(a) but only differs from figure 4(a) in which low T and h values, the $F_{3/2} + FQ$ phase or coexistence region also exist. The dynamic phase boundary between this $F_{3/2} + FQ$ region and the $F_{3/2}$ phase is the first-order line. (iii) For $k = 0.5$ and $d = 0.125$, the phase diagram is

illustrated in figure 4(c), and it is similar to case (ii), except that the $F_{3/2}+F_{1/2}$ phase occurs for very low values of T and h. The dynamic phase boundary between the $F_{3/2}+F_{1/2}$ phase and the $F_{3/2}$ phase is also a first-order line. (iv) For $k=0.1$ and $d=-0.375$, the phase diagram is presented in figure 4(d). While this phase diagram has the same phase topology as the diagram in figure 4(c), it differs from figure 4(c) in which the $F_{3/2}+F_{1/2}$ and $F_{3/2}+FQ$ phases or coexistence regions become large and in a certain range of h they overlap each other, hence one more coexistence region, namely the $F_{3/2}+F_{1/2}+FQ$ phase also exists. The dynamic phase boundaries among these coexistence regions are all first-order lines. (v) For $k=0.5$ and $d=-0.25$, the calculated phase diagram is illustrated in figure 4(e). This is the more interesting phase diagram in which the system exhibits the dynamic double critical end point (B), the dynamic tricritical point and five coexistence regions or phases, namely $F_{3/2}+F_{1/2}$, $F_{3/2}+F_{1/2}+FQ$, $F_{3/2}+FQ+D$, $F_{3/2}+FQ$, and $F_{3/2}+D$. The dynamic boundaries between these coexistence phases are first-order lines, except the boundary between the $F_{3/2}+F_{1/2}$ and $F_{3/2}+FQ$ phases; this boundary is a second-order line. This phase diagram also exhibits the dynamic double critical end point (B), where two critical phases coexist, which occurs for high values of T and h. (vi) For $k=0.5$ and $d=-0.375$, the phase diagram is seen in figure 4(f). This phase diagram is very similar to figure 4(e), except that the $F_{3/2}+D$ phase disappears and the $FQ+D$ phase occurs for low values T and high values of h. (vii) This type of phase diagram is presented for $k=1.0$ and $d=-0.25$, seen in figure 4(g), and is similar to figure 4(f) but only differs from figure 4(f) in that the $F_{3/2}+FQ+D$ phase region disappears and the $FQ+D$ phase region becomes large. (viii) We show the phase diagram for $k=0.5$ and $d=-1.0$, seen in figure 4(h). This is also an interesting phase diagram in which the $F_{1/2}$ and $F_{1/2}+FQ$ phases occur and the dynamic phase boundary between the $F_{1/2}$ phase and the D phase is a second-order line, boundaries among the $F_{1/2}$ phase and the coexistence phase regions are first-order lines. Moreover, the $FQ+D$ phase becomes smaller. (ix) The phase diagram is constructed for $k=0.5$ and $d=-1.25$, seen in figure 4(i), and is similar to figure 4(h) but differs from figure 4(h) in that the $F_{3/2}+F_{1/2}$ and $F_{3/2}+F_{1/2}+FQ$ phase regions disappear.

In figure 5, two dynamic tricritical points exist and only two fundamental phase diagrams are found. (i) For $k=2.0$ and $d=-0.125$, the phase diagram is seen in figure 5(a). In this phase diagram, besides two dynamic tricritical points and a dynamic double critical end point, where the D and $FQ+D$ critical phases coexist, the D phase and four coexistence regions or phases, namely $F_{3/2}+F_{1/2}$, $F_{3/2}+F_{1/2}+FQ$, $F_{3/2}+FQ$, and $FQ+D$, exist in the system. The dynamic phase boundaries among these phases are first-order lines, except the boundary between the $F_{3/2}+F_{1/2}$ and $F_{3/2}+FQ$ phases, and between the $F_{3/2}+FQ$ and $FQ+D$ phases, that are second-order lines, seen in the figure. (ii) This type of phase diagram is presented for $k=2.0$ and $d=1.25$, seen in figure 5(b), and is similar to figure 5(a) but differs from figure 5(a) in that the $FQ+D$ phase region disappears and the $F_{3/2}$ and $F_{3/2}+D$ phases occur. The dynamic phase boundary between the $F_{3/2}$ phase and D phase is a second-order line, but the boundaries among the $F_{3/2}$, $F_{3/2}+D$, and $F_{3/2}+FQ$ phases are all first-order lines.

In figure 6, three dynamic tricritical points exist and the following six main topological different types of phase diagrams are found. (i) For $k=0.1$ and $d=-0.50$, the phase diagram is illustrated in figure 6(a), and besides the $F_{1/2}$ and D phases the system exhibits four coexistence regions or phases, namely $F_{3/2}+F_{1/2}$, $F_{3/2}+F_{1/2}+FQ$, $F_{3/2}+FQ$, and $F_{1/2}+FQ$. The dynamic boundaries among these coexistence phases are all first-order lines, except the boundary between the $F_{3/2}+F_{1/2}$ and $F_{3/2}+FQ$ phases, that is a second-order line. Moreover, the boundary between the $F_{1/2}$ and D phases is also a second-order line in which occurs for high values of h. Since the boundary between the $F_{3/2}+F_{1/2}$ and $F_{3/2}+F_{1/2}+FQ$ phases for low values of T and h is a first-order line, one dynamic tricritical point occurs. On the other hand,

the second-order phase line, that occurs at high values of h and separates the $F_{1/2}$ phase from the D phase, has a bulge and suggests the occurrence of some sort of re-entrant phenomenon, because as the h values increase the system passes from the ordered phase to the disordered phase and then passes from the disordered (D) phase to the ordered phase, and finally back to the D phase again. At both ends of this second-order line two dynamic tricritical points exist, because the two boundaries between the $F_{1/2}$ and $F_{1/2}+FQ$ phases, one for low values of T and for high values of h, are first-order lines. (ii) For $k = 0.1$ and $d = -0.625$, the phase diagram is seen in figure 6(b). This phase diagram is very similar to figure 6(a) for high values of h, but for low values of h the $F_{1/2}$ phase and $F_{1/2} + FQ$ coexistence phase region occur. The dynamic phase boundary between the $F_{1/2}$ phase and D phase is a second-order line for high values of T and the other lines are first-order lines for low values of T and h, therefore a dynamic tricritical point occurs in this region. (iii) For $k = 0.1$ and $d = -0.7125$, the phase diagram is illustrated in figure 6(c), and it is similar to figure 6(b), except that the $F_{3/2} + F_{1/2}$ phase region becomes smaller and the $F_{3/2} + F_{1/2} + FQ$ phase disappears. (iv) The phase diagram is presented for $k = 0.1$ and $d = -1.0$, seen in figure 6(d), and is similar to figure 6(c) but differs from figure 6(c) in that the $F_{3/2}+F_{1/2}$ phase region disappears and the $F_{1/2}+FQ$ phases that exist for high values of h become smaller. (v) The phase diagram is obtained for $k = 0.5$ and $d = -0.125$, seen in figure 6(e). This is one of the more interesting phase diagrams in which the system exhibits three dynamic tricritical points and also five coexistence regions or phases, namely $F_{3/2} + F_{1/2}$, $F_{3/2} + F_{1/2} + FQ$, $F_{3/2} + FQ$, $F_{3/2} + FQ + D$ and $F_{3/2} + D$ and also D phase. The dynamic boundaries among these phases are first-order lines, except the boundaries between the $F_{3/2} + F_{1/2}$ and $F_{3/2} + FQ$ phases, and between the $F_{3/2}$ and D phase; these boundaries are second-order lines. This phase diagram is very similar to figure 6(a) for low values of h and T, but for high values of h the $F_{1/2}$, $F_{1/2} + FQ$ phases and the bulge on the second-order phase line disappear. Moreover, the $F_{3/2} + FQ$ phase becomes large and the $F_{3/2} + D$ phase appears for high values of h and low values of T. Furthermore, one more $F_{3/2}+D$ phase occurs for high values of T and low values of h. The dynamic phase boundaries between the $F_{3/2} + D$ and $F_{3/2}$ phases, and between the $F_{3/2} + D$ and D phases, are first-order lines, and these lines start $h = 0.0$ and merge at one of the dynamic tricritical points, seen in the figure; compare figures 6(a) and (e). (vi) For $k = 1.0$ and $d = 0.125$, the phase diagram is given in figure 6(f). While this phase diagram has the same phase topology as the diagram in figure 6(e), it differs from figure 6(e) in that the $F_{3/2} + FQ + D$ phase disappears and the $FQ + D$ phase occurs for high values of h and low values of T.

6. Summary and discussion

We have analysed within a mean-field approach the stationary states of the kinetic spin-3/2 BEG model. We use a Glauber-type stochastic dynamics to describe the time evolution of the system. We have studied the behaviour of the time-dependence dynamic order parameters, namely magnetization or the dipole moment and the quadrupole moment in a period, also called the dynamic magnetization and dynamic quadrupole moment, as a function of reduced temperature. The DPT points are found by investigating the behaviour of the dynamic order parameters in a period as a function of the reduced temperature. These investigations are also checked and verified by calculating the Liapunov exponents. Finally, we present the phase diagrams in the (T, h) plane. We found that the behaviour of the system strongly depends on the values of k and d and 17 different phase diagram topologies are found. The phase diagrams exhibit the D, $F_{3/2}$, $F_{1/2}$, and/or $F_{3/2} + F_{1/2}$, $F_{3/2} + D$, $F_{3/2} + F_{1/2} + FQ$, $F_{3/2} + FQ$, $F_{1/2} + FQ$, $F_{3/2} + FQ + D$, and/or $FQ + D$ coexistence regions depending on k and d values and the dynamic phase boundaries among these phases and coexistence regions are mostly first-order

lines, except the boundaries between the $F_{3/2}$ and D phases and between the $F_{1/2}$ and D phases; these boundaries are second-order lines, seen in figures 4–6. Moreover, the dynamic phase boundary between the $F_{3/2} + F_{1/2}$ and $F_{3/2} + FQ$ phases is also a second-order line. Therefore, one, two, or three dynamic tricritical points and a dynamic double critical end point also occur, that depend on k and d values. Finally, we also mention that we have also calculated the Liapunov exponents to verify the stability of the solutions and the DPT points.

Finally, since we found the 17 different phase diagram topologies in the kinetic spin-3/2 BEG model, this system gives more complex and richer phase diagrams than in the kinetic spin-1 BC, and kinetic isotropic BEG models, as well as in the kinetic spin-3/2 BC model. For example, in the kinetic spin-1 BC model [31] we have found five main different types of phase diagrams; for the kinetic spin-1 isotropic BEG model [32] and spin-3/2 BC model [27] the six fundamental types of phase diagrams are obtained. On the other hand, in the present system, the phase diagrams exhibit seven coexistence phase regions besides one disordered and two ordered phases depending on k and d values, but for the spin-1 BC model the phase diagrams exhibit one coexistence phase region besides one disordered and one ordered phase depending only on d values; for the spin-1 isotropic BEG model the phase diagrams exhibit three coexistence phase regions besides the disordered and the ordered phase; for the spin-3/2 BC model the phase diagrams exhibit four coexistence phase regions besides the one disordered and two ordered phases depending on d values. Moreover, only one phase diagram, namely figure 4(a), is obtained in the present model, which is similar to one of the phase diagrams which has been found in the above mentioned models as well as in the kinetic spin-1/2 Ising model, that only one type of phase diagram was obtained for the spin-1/2 model, and hence it is similar to figure 4(a) [29]. Furthermore, in this model in some cases three dynamic tricritical points occur, whereas one or two dynamic tricritical points appear in the above mentioned models.

Acknowledgments

This work was supported by the Technical Research Council of Turkey (TÜBİTAK), grant No 105T114, and Erciyes University Research Funds, grant No FBA-06-01.

References

[1] Sivardière J and Blume M 1972 *Phys. Rev.* B **5** 1126
[2] Bakchich A, Bassir A and Benyuossef A 1993 *Physica* A **195** 188
Tsushima N and Honda Y 1998 *J. Phys. Soc. Japan* **67** 1574
[3] Kaneyoshi T and Jaščur M 1993 *Phys. Lett.* A **177** 172
[4] Tsushima N, Honda Y and Horiguchi T 1997 *J. Phys. Soc. Japan* **66** 3053
[5] Albayrak E and Keskin M 2002 *J. Magn. Magn. Mater.* **241** 249
[6] Sâ Barreto F C and De Alcantara Bonfim O F 1991 *Physica* A **172** 378
[7] Bakkali A, Kerouad M and Saber M 1996 *Physica* A **229** 563
[8] Tucker J W 2000 *J. Magn. Magn. Mater.* **214** 121
[9] Backhich A and El Bouziani M 2001 *J. Phys.: Condens. Matter* **13** 91
[10] Ekiz C, Albayrak E and Keskin M 2003 *J. Magn. Magn. Mater.* **256** 311
[11] Ekiz C 2004 *Phys. Status Solidi* b **241** 1324
[12] Keskin M, Pınar M A, Erdinç A and Canko O 2006 *Physica* A **364** 263
[13] Kaneyoshi T and Jaščur M 1992 *Phys. Status Solidi* b **173** K37
Le Gal G, Kaneyoshi T and Khater A 1993 *Physica* A **195** 174
Peliti L and Saber M 1996 *Phys. Status Solidi* b **195** 537
[14] Plascak J A, Moreira J G and Să Barreto F C 1993 *Phys. Lett.* A **173** 360
[15] Ilkovič V 1996 *Physica* A **234** 545

[16] Xavier J C, Alcaraz F C, Lara D P and Plascak J A 1998 *Phys. Rev.* B **57** 11575
[17] Lara D P and Plascak J A 1998 *Int. Mod. Phys.* B **12** 2045
[18] Grollau S 2002 *Phys. Rev.* E **65** 056130
[19] Plascak J A and Landau D P 2003 *Phys. Rev.* E **67** 015103(R)
[20] Özsoy O, Albayrak E and Keskin M 2002 *Physica* A **304** 443
[21] Bakchich A, Bekhechi S and Benyoussef A 1994 *Physica* A **210** 415
[22] Bekhechi S and Benyoussef A 1997 *Phys. Rev.* B **56** 13954
[23] Ekiz C 2004 *Phys. Lett.* A **325** 99
[24] Ekiz C 2004 *J. Magn. Magn. Mater.* **284** 409
[25] Keskin M, Pınar M A, Erdinç A and Canko O 2006 *Phys. Lett.* A **353** 116
[26] Grandi B C S and Figueiredo W 2004 *Phys. Rev.* E **70** 056109
[27] Keskin M, Canko O and Deviren B 2006 *Phys. Rev.* E at press
[28] Glauber R J 1963 *J. Math. Phys.* **4** 294
[29] Tomé T and de Oliveira M J 1990 *Phys. Rev.* A **41** 4251
[30] Buendía G M and Machado E 1998 *Phys. Rev.* E **58** 1260
[31] Keskin M, Canko O and Temizer Ü 2005 *Phys. Rev.* E **72** 036125
[32] Keskin M, Canko O and Kantar E 2006 *Physica* A submitted
[33] Mendes J F F and Lage E J S 1991 *J. Stat. Phys.* **64** 653
[34] Acharyya M 1997 *Phys. Rev.* E **56** 2407
Chatterjee A and Chakrabarti B K 2003 *Phys. Rev.* E **67** 046113
[35] Sides S W, Rikvold P A and Novotny M A 1998 *Phys. Rev. Lett.* **81** 834
Sides S W, Rikvold P A and Novotny M A 1999 *Phys. Rev.* E **59** 2710
Korniss G, White C J, Rikvold P A and Novotny M A 2001 *Phys. Rev.* E **63** 016120
Korniss G, Rikvold P A and Novotny M A 2002 *Phys. Rev.* E **66** 056127
[36] Chakrabarti B K and Acharyya M 1999 *Rev. Mod. Phys.* **71** 847
[37] Krawiecki A 2005 *Int. J. Mod. Phys.* B **19** 4769
[38] Zimmer M F 1993 *Phys. Rev.* E **47** 3950
Acharyya M and Chakrabarti B K 1995 *Phys. Rev.* B **52** 6550
Acharyya M 1998 *Phys. Rev.* E **58** 179
Fujisaka H, Tutu H and Rikvold P A 2001 *Phys. Rev.* E **63** 036109
[39] Tutu H and Fujiwara N 2004 *J. Phys. Soc. Japan* **73** 2680
[40] Khorrami M and Aghamohammadi A 2002 *Phys. Rev.* E **65** 056129
[41] Jiang Q, Yang H N and Wang G C 1995 *Phys. Rev.* B **52** 14911
Jiang Q, Yang H N and Wang G C 1996 *J. Appl. Phys.* **79** 5122
[42] Kleemann W, Braun T, Dec J and Petracic O 2005 *Phase Transit.* **78** 811
[43] Jang H and Grimson M J 2001 *Phys. Rev.* E **63** 066119
Jang H, Grimson M J and Hall C K 2003 *Phys. Rev.* B **67** 094411
Jang H, Grimson M J and Hall C K 2003 *Phys. Rev.* E **68** 046115
[44] Yasui T, Tutu H, Yamamoto M and Fujisaka H 2002 *Phys. Rev.* E **66** 036123
Yasui T, Tutu H, Yamamoto M and Fujisaka H 2003 *Phys. Rev.* E **67** 019901 (erratum)
[45] Machado E, Buendía G M, Rikvold P A and Ziff R M 2005 *Phys. Rev.* E **71** 016120
[46] Acharyya M 2005 *Int. J. Mod. Phys.* C **16** 1631